

## Dielectric response of hydrated water as a structural component of nanofibrillated cellulose (NFC) from different plant sources

Ivan Lunev<sup>a,b</sup>, Anna Greenbaum (Gutina)<sup>c,d</sup>, Yuri Feldman<sup>c</sup>, Vladimir Petrov<sup>e</sup>, Nina Kuznetsova<sup>e</sup>, Natalia Averianova<sup>e</sup>, Olga Makshakova<sup>a</sup>, Yuriy Zuev<sup>a,b,\*</sup>

<sup>a</sup> Kazan Institute of Biochemistry and Biophysics, FRC Kazan Scientific Center of RAS, Lobachevsky Str. 2/31, 420111, Kazan, Russian Federation

<sup>b</sup> Kazan Federal University, Kremlyovskaya str., 18, 420008, Kazan, Russian Federation

<sup>c</sup> The Hebrew University of Jerusalem, Department of Applied Physics, Edmond J. Safra Campus, Jerusalem 9190401, Israel

<sup>d</sup> The Hebrew University of Jerusalem, Racah Institute of Physics, Edmond J. Safra Campus, Jerusalem 9190401, Israel

<sup>e</sup> Kazan National Research Technological University, Karl Marx Str. 68, 420015, Kazan, Russian Federation

### ARTICLE INFO

#### Keywords:

Nanofibrillated cellulose  
Films  
Hydrated water  
Dielectric spectroscopy

### ABSTRACT

The current work illuminates the interplay between nanofibrillated cellulose (NFC) films and hydrated water. The NFC films from three sources of technological importance, i.e. cotton, wood and flax, are compared. It is shown that cellulose materials present slight variations in supramolecular structure depending on the plant origin. The structural differences determine both quantity and state of the water adsorbed by cellulose. Dielectric spectroscopy was employed to study the state of hydrated water as a probe of both the overall and specific marks of NFCs' structure. The measurements, carried out in the wide frequency ( $10^{-2}$  Hz– $10^6$  Hz) and temperature (123 K–293 K) ranges, revealed the formation of non-interactive water clusters at low water content. At high water content, additional states of water were identified: Water in saturated glass-forming solution and bulk. These water states were shown to be determined by the NFC's structure and morphology.

### 1. Introduction

Plants are one of the main primary bases for human life, used either directly or indirectly in manufactured form, to provide food, energy, shelter, and medicine (Rankoana, 2016). The use of natural materials has increased significantly through the development of new processes and products based on these materials. Thus, the information on their structure and properties is very important.

Cellulose is one of the most significant components in the plant cell wall, abundantly represented in both its thin primary and thick secondary layers. The cellulose macromolecule is a linear 1,4  $\beta$ -glucan (Fig. 1).

*In planta*, cellulose macromolecules are synthesized at the plasma membrane by the cellulose synthase complex consisting of 18 glycosyltransferases (Nixon et al., 2016). Once synthesized, cellulose macromolecules interact with each other in parallel orientation (cellulose I) and form bundles of a diamond-shape pattern, where, according to recent findings, 18 chains can be assembled in 5 layers in the 34,443

arrangement (Kubicki et al., 2018). These bundles, called elementary fibrils or microfibrils in higher plants, have a cross section of 3–4 nm (Pérez & Mazeau, 2005). The elementary fibrils are further stacked in large, supramolecular bundles with a transverse width from dozens to hundreds of nanometers (Fengel, 1971). The hierarchical organization of cellulose fibrils is shown in Fig. 1. The well-known two-phase cellulose model depicts cellulose chains containing both ordered crystalline and less-ordered amorphous domains (Nisizawa, 1973).

One of the promising uses of cellulosic materials is their application in the so-called nanofibrillated state (nanofibrillated cellulose or NFC), which is sometimes referred to as microfibrillated cellulose (Belbekhouche et al., 2011; Chinga-Carrasco, 2011). In NFC the cellulose fibers are mechanically degraded to create aggregates of cellulose elementary fibrils with a nanoscale diameter of 20–100 nm and a length of several micrometers (sometimes called nanofibrils) (Lavoine, Desloges, Dufresne, & Bras, 2012). Note that the fine structure of the NFC strongly depends on both the protocol of the mechanical treatment (Iwamoto, Nakagaito, & Yano, 2007) and the origin of the cellulose

\* Corresponding author at: Kazan Institute of Biochemistry and Biophysics, FRC Kazan Scientific Center of RAS, Lobachevsky Str. 2/31, 420111, Kazan, Russian Federation.

E-mail addresses: [lunev75@mail.ru](mailto:lunev75@mail.ru) (I. Lunev), [anechka@mail.huji.ac.il](mailto:anechka@mail.huji.ac.il) (A. Greenbaum (Gutina)), [yurif@mail.huji.ac.il](mailto:yurif@mail.huji.ac.il) (Y. Feldman), [ptrv@kstu.ru](mailto:ptrv@kstu.ru) (V. Petrov), [kznina@gmail.com](mailto:kznina@gmail.com) (N. Kuznetsova), [natalia.v.averianova@gmail.com](mailto:natalia.v.averianova@gmail.com) (N. Averianova), [olga.makshakova@kibb.knc.ru](mailto:olga.makshakova@kibb.knc.ru) (O. Makshakova), [zuev@kibb.knc.ru](mailto:zuev@kibb.knc.ru) (Y. Zuev).

<https://doi.org/10.1016/j.carbpol.2019.115217>

Received 7 May 2019; Received in revised form 15 August 2019; Accepted 19 August 2019

Available online 19 August 2019

0144-8617/ © 2019 Published by Elsevier Ltd.

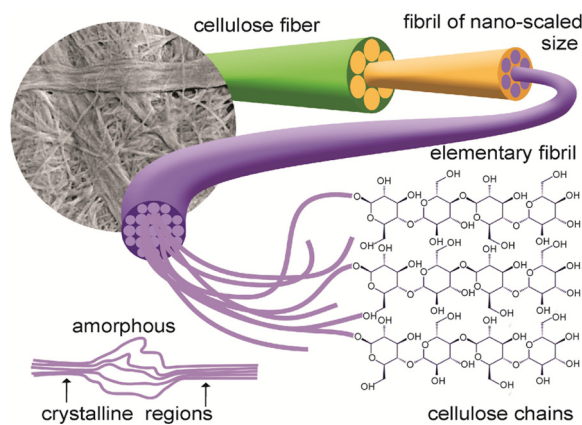


Fig. 1. Scheme of the supramolecular hierarchical organization of cellulose.

(Alemdar & Sain, 2008; Heux, Dinand, & Vignon, 1999; Siqueira, Bras, & Dufresne, 2010). Owing to a particularly large surface area, a large amount of hydroxyl groups and fibril flexibility, the suspension of nanofibrillated cellulose forms a viscous thinning aqueous gel (Charreau, Foresti, & Vázquez, 2013; Lu, Askeland, & Drzal, 2008), where the polymer network is stabilized by water and interfibrillar hydrogen bonds. In the course of drying, the NFC gels form porous films whose technological properties are determined by the amount of water-binding centers and their accessibility for water.

The content and properties of water in cellulose samples are of crucial importance for a range of technological applications, such as food packaging, paper printing, etc. (Lavoine et al., 2012; Viet, Beck-Candanedo, & Gray, 2007). For example, the competitive hydrogen bonding of cellulose with water causes a disruption in percolated NFC networks, resulting in remarkable material softening (Dagnon, Shanmuganathan, Weder, & Rowan, 2012.).

In the present study, we analyzed the specific properties of water located in NFC films derived from three technologically important plant sources (wood, cotton and flax). We performed an extensive dielectric study of absorbed water by NFCs of different plant origins over a wide frequency and temperature range.

Recently, unique physical and chemical properties of water have been noted under the influence of different molecular interfaces, depending on their structure and dynamics (Chen et al., 2014; Ehre, Lavert, Lahav, & Lubomirsky, 2010; Gallo, Rovere, & Chen, 2012; Reiter et al., 2013). For example, the nucleation and crystallization temperature of hydrated water show a strong dependency on the type of interface in contact with the water (Ehre et al., 2010). Furthermore, the nanoconfined water has been found to have transport and thermodynamic properties that differ from those of the bulk (Suzuki, Duran et al., 2015; Suzuki, Steinhart, Butt, & Floudas, 2015). The unique properties of the confined/bound water are determined by the specific nature of the confining space, including its volume, the structure of limiting boundaries and the specifics of the H-bond network (Lang & Ludemann, 1982; Stokely, Mazza, Stanley, & Franzese, 2010; Tanaka, 2013). The hydration shell of various natural and synthetic macromolecules have been studied extensively over the last several decades with a variety of experimental techniques (Bone & Pethig, 1982; Martin & Matyushov, 2015; Pal, Peon, & Zewail, 2002; Rupley, Gratton, & Careri, 1983). The different states of hydration/interfacial water span an extremely wide range of characteristic time-scaled processes. One of the most versatile experimental methodologies capable of concurrently addressing a wide range of time/frequency scales is the Broadband Dielectric Spectroscopy (BDS) (Feldman, Ermolina, & Hayashi, 2003; Feldman, Puzenko, & Ryabov, 2006; Kremer & Schonhals, 2003). It presently covers an enormous frequency range, from  $\sim 10^{-6}$  Hz to  $\sim 10^{12}$  Hz, enabling a practical study of the complete spectrum of dielectric relaxation phenomena. This method is particularly relevant for polar

mediums such as water and water-solvated samples. To study different populations of water via dielectric polarization, the system must be quenched or placed in a regime of tight confinement (Feldman, Puzenko, Ben Ishai, & Gutina Greenbaum, 2014). In this case, the water can be considered to be a dipole sub-system, while the other components may be defined as the matrix (Feldman et al., 2014).

Recently, dielectric spectroscopy studies of different polysaccharides have been reported in the literature: Cellulose (Einfeldt & Kwasniewski, 2002; Jafarpour, Dantras, Boudet, & Lacabanne, 2007; Jafarpour, Roig, Dantras, Boudet, & Lacabanne, 2009; Roig, Dantras, Dandurand, & Lacabanne, 2011; Zhao, Chen, Du, & Chen, 2019), various cellulose derivatives (Einfeldt, Meißner, & Kwasniewski, 2003; Rachocki, Markiewicz, & Tritt-Goc, 2005) and cellulose nano- or microcrystalline structures (Bras, Strømme, & Mihranyan, 2015; Nilsson, Frenning, Gråsjö, Alderborn, & Strømme, 2006; Sousa et al., 2010). However, the specific correlations obtained between the dielectric characteristics and the structural, physical and chemical properties of the materials studied have only a particular significance since they do not permit an overview of the generalized structural model of cellulose properties. The dielectric studies of water, which is present in all cellulose materials and displays both the overall and specific marks of their structure, can serve as a universal approach to characterize the generalized structural properties of cellulose samples. In the present work, on the basis of the approach developed for water adsorbed onto hydrated proteins (Kurzweil-Segev, Gutina, Popov, Golodnitsky, & Feldman, 2016; Kurzweil-Segev, Popov, Eisenberg et al., 2017; Kurzweil-Segev, Popov, Eisenberg et al., 2017), we will show that the generalized morphology of the NFC matrix influences the nature of dielectric polarization of hydrated water due to the dynamic interactions between water and binding or conjunctive centers of the cellulose matrix. Thus, the state of hydrated water and consequently its dielectric properties will be strongly determined by the morphology of the porous NFC films.

## 2. Experimental

### 2.1. Materials

#### 2.1.1. Raw materials

The raw materials used were commercially available cellulose fibers from cotton, wood and flax. The bleached softwood kraft pulp (BSKP) was obtained from CMPC Celulosa S.A., Chile. The cotton lint cellulose of the highest quality was from Medicot, Uzbekistan. Blast fibers of flax plants were the gift from All-Russian Research Institute for Flax, Torzhok, Russia.

#### 2.1.2. NFC production

All samples were pre-crushed using the Pulverisette 15 cutting mill, rotor speed 3000 rev/min. The grinding time was 5 min; a sieve with a mesh size of 0.25 mm was used. The resulting suspensions were defibrillated by passing them through an APV2000-Lab homogenizer operated at 110 MPa pressure. The nanofibrillated material was collected after 30 passes through the homogenizer. The nanofibrillated cellulose water suspensions (0.5%) were allowed to dry in Petri dishes at room temperature and humidity.

### 2.2. Wide-angle X-ray diffraction

The X-ray phase studies of the NFC films were performed on an Ultima IV RIGAKU automatic X-ray diffractometer equipped with a theta-theta goniometer, using  $\text{CuK}\alpha$  radiation (40 kV, 40 mA) via a Ni K- $\beta$  filter ( $\lambda = 1.5418 \text{ \AA}$ ). The data was collected in reflection mode with a flat-plate sample at 23 °C. The samples in the diffractometer were placed in arbitrary orientations and were centered at the goniometer optical center. The X-ray patterns were recorded in the  $2\theta$  range between 6 and 50°, in 0.01° steps, with a scan rate of 1°/min. The resulting

X-ray patterns were processed with PDXL software. The main structural characteristics were calculated on the basis of the diffraction patterns. The crystallinity index was calculated as the ratio of the area under the curve pertaining to crystalline structures to the area under the sum of the crystalline and amorphous structures.

The crystallite size was calculated using the Scherrer equation:  $L = k \lambda / \beta \cos \theta$ , where  $L$  is the effective size of the crystallite in Å,  $\lambda$  is the X-ray wavelength in Å,  $\theta$  is the Bragg angle in degrees,  $k$  is the coefficient, taking into account the crystallite shape and  $\beta$  is the line width in radians.

### 2.3. Atomic force microscopy

The NFC surface morphology was studied using a MultiMode-5 atomic force microscope (Bruker, Germany) with a Nanoscope V controller. The sample was prepared by dripping 10 µl of the ultra-sonificated solution of MFC particles into deionized water and drying for 2 min. All the images were obtained using the ScanAsyst regime. A rectangular cantilever RTESP (Veeco) with silicon tip was used. The image resolution was 512 × 512 points at the scan speed of rate 1 Hz. The microphotographs thus obtained were analyzed using the program ImageJ.

### 2.4. Dielectric spectroscopy

Dielectric measurements in the frequency range of 10<sup>-2</sup> Hz – 10<sup>6</sup> Hz were performed using a Broadband Dielectric Spectrometer, BDS Concept 80, based on the Alpha Impedance Analyzer (Novocontrol Technologies GmbH & Co. KG) with automatic temperature control by a QUATRO Cryosystem.

For the dielectric experiments, the NFC films were treated for 48 h under a vacuum of 0.8 bar, and then placed into a desiccator with controlled steam humidity. The films were kept overnight at 25 °C in an atmosphere of saturated CaCl<sub>2</sub>·6H<sub>2</sub>O water solution (~29% relative humidity) (Richardson & Malthus, 1955) and K<sub>2</sub>SO<sub>4</sub> (~98%) (Arai, Hosaka, & Murase, 1976), to obtain samples with low and high hydration levels.

Next, the materials were mounted between two electrodes forming the plate capacitor sample cell. The parallel plate capacitor configuration consisted of two 16 mm-diameter electrodes spaced 0.5 mm apart. The measurements were carried out using the following protocol: Each sample was placed into the measuring cell at room temperature and then quenched down to temperature 123 K at a rate of 12 K/min. The samples were then heated and measured at intervals of 3 K up to 293 K. The accuracy of the complex dielectric permittivity measurement was better than 3%.

## 3. Results and discussion

### 3.1. Samples crystallinity

The X-ray diffraction patterns of three NFC films (Fig. 2) are typical for cellulose I (Abou-Sekkina, Sakran, & Saafan, 1986). There are three peaks at  $2\theta = 14.8^\circ$ ,  $16.4^\circ$  and  $22.8^\circ$ , which correspond to the (1 $\bar{1}$ 0), (110) and (200) planes, respectively (Wada, Okano, & Sugiyama, 1997; Wada, Sugiyama, & Okano, 1993). The main structural characteristics of NFC films are summarized in Table 1. The peak at  $22.8^\circ$ , attributed to the transverse size of the fibril, allowed us to calculate the d-spacing, which amounted to 3.9 Å. The crystallite size varies from 40 to 41 Å for flax and wood to 53 Å for cotton NFC. These values are in good agreement with the known transverse size of microfibrils in plant cellulose (Pérez & Mazeau, 2005). Another distinction regarding the value of the NFC crystallinity index is that it is lower (76–77%) for flax and wood than for cotton (86%).

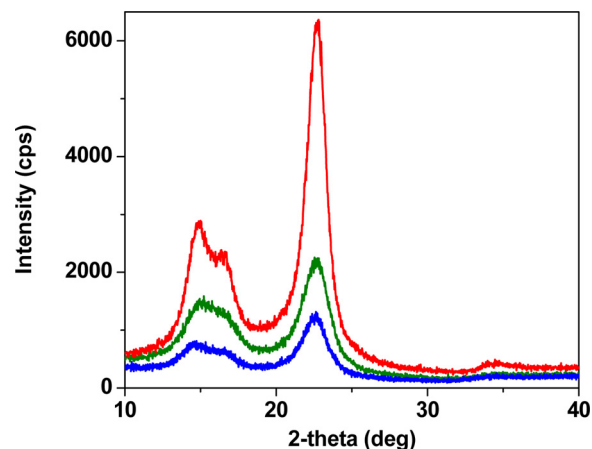


Fig. 2. X-ray diffraction patterns of NFC films from cotton (upper curve), wood (middle) and flax (lower curve). (For interpretation of the references to colour in this figure legend, the reader is referred to the web version of this article.)

Table 1

Some structural characteristics of NFCs from wood, flax and cotton obtained by wide-angle X-ray diffraction.

	Planes	d-spacing, Å	Effective crystallite size (L), Å	Crystallinity index, %
Wood	(1 $\bar{1}$ 0)	6.0	32	77
	(110)	5.3	39	
	(200)	3.9	40	
Flax	(1 $\bar{1}$ 0)	6.1	40	76
	(110)	5.3	47	
	(200)	3.9	41	
Cotton	(1 $\bar{1}$ 0)	6.0	45	86
	(110)	5.3	69	
	(200)	3.9	53	

### 3.2. Ultrastructure of NFC

Atomic-force microscopy of the studied samples revealed that NFC bundles of samples differ with respect to the transverse size of the fibrils (Fig. 3). The transverse size of fibrils after homogenization varied between 20–150 nm, which corresponds to the average diameter of nanofibrils in the samples: 48 nm for cotton, 68 nm for wood and 135 nm for flax, which were obtained using the ImageJ image analysis software. Assuming the nanofibril is a cylinder, based on its diameter and simple geometrical arguments, one can estimate the ratio between the surface area of one nanofibril of unit length for flax, wood and cotton, to that of cotton as 2.8/1.4/1. Assuming the uniform distribution of the hydroxyl groups across the cellulose chain, we can state that the ratio of surface groups to those in the fibril volume is higher for fibrils of lesser diameter. Therefore, under the approximately similar density of the different NFC films we can estimate the ratio of total hydroxyls exposed at the surface to the buried ones as 0.35/0.7/1 for flax, wood and cotton.

### 3.3. Water uptake by NFC films

The water fraction in the samples (Table 2) was calculated as  $h = M_w/M_d$ , where  $M_w$  and  $M_d$  are the weight of water and dry sample, respectively. Overall, the water uptake values for the NFC films studied fit well with those reported previously for sisal NFC (Belbekhouche et al., 2011). The water uptake at 29% and 98% relative humidity corresponds to distinct water sorption processes. At 29% steam humidity, water molecules predominantly adsorb directly onto the hydroxyl groups of the external surfaces and in the low-ordered amorphous regions, forming the so-called first hydration layer, while at 98% relative humidity swelling of the NFC film occurs (Belbekhouche et al.,

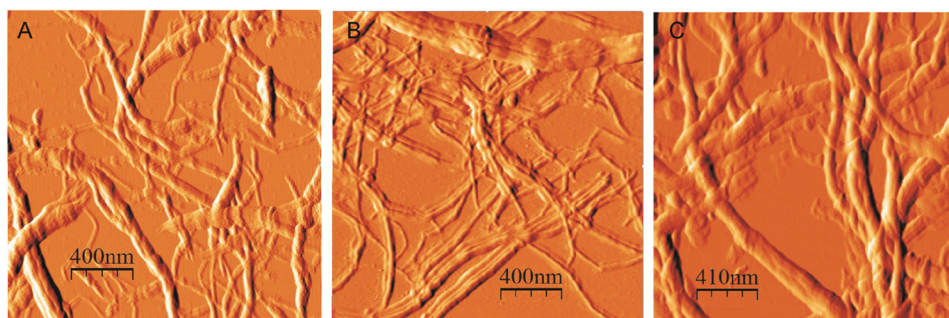


Fig. 3. Atomic force microphotographs of NFC from cotton (A), wood (B) and flax (C).

Table 2

Water uptake at different relative humidity.

Relative humidity, %	Water fraction (h), g/g		
	Cotton	Wood	Flax
29	0.09 ± 0.01	0.08 ± 0.01	0.03 ± 0.01
98	0.29 ± 0.02	0.28 ± 0.02	0.23 ± 0.03

2011).

The NFC films from cotton, wood and flax demonstrate variations in water sorption at the same relative humidity. Thus, the flax NFC films adsorb the least amount of water compared with wood and cotton. The ratio between water fractions of flax and cotton NFC films at 29% relative humidity has a factor of 0.33. Assuming uniform distribution of hydroxyl centers over the fibril surface, we can see a correlation between water uptake and the fibril dimensions. As previously documented, the ratio of the surface areas of cotton and flax NFC is 0.35. Thus, according to our volumetric qualifications and the water uptake data presented in Table 2, we see that for cotton and flax the amount of fibril surface accessible for solvent is related to their surface area. The cotton and wood samples demonstrate almost equal water uptake, which could be due to the compensation of two opposite factors that determine the amount of adsorbed water in NFC films: the ratio of the crystalline and amorphous regions (crystallinity index) and the fibril thickness.

### 3.4. Dielectric spectroscopy

#### 3.4.1. Relaxation processes of NFC hydrated water

The typical dielectric loss spectra of hydrated NFC from wood versus frequency and temperature are presented in Fig. 4. Several relaxation processes at different frequencies and temperature intervals describe the dielectric response of all the NFC samples. The relaxation process LT<sub>1</sub> (the first low-temperature process), is observed for all of the

samples studied at low hydration levels in the temperature region below 200 K (Figs. 4a and b). At high hydration levels we see two separate relaxation processes, LT<sub>1</sub> and LT<sub>2</sub> (a second low-temperature process) (Fig. 4b). At higher temperatures, a relaxation process with a specific saddle-like shape is detected for all NFCs with different water contents (Fig. 4). The percolation process is easily detected at temperatures around 280 K (Puzenko, Kozlovich, Gutina, & Feldman, 1999). For some samples equilibrated under water vapor, a well-defined ice melting phase transition is clearly detected (see Fig. 4b) (Kurzweil-Segev, Popov, Eisenberg et al., 2017; Popov, Puzenko, Khamzin, & Feldman, 2015). In this work, we will discuss in detail only the low-temperature processes observed for all of the studied samples at both hydration levels. We will provide the analyses of these processes in NFC hydrated films in the framework of the approach developed for water adsorbed in hydrated proteins (Kurzweil-Segev et al., 2016; Kurzweil-Segev, Popov, Eisenberg et al., 2017; Kurzweil-Segev, Popov, Sagit, Solomonov, & Feldman, 2017).

Several states of water can be detected in the hydrated heterogeneous systems using various methods (Kurzweil-Segev et al., 2016). It was shown that at hydration rates  $0.07 < h < 0.2$  (samples prepared at 29% humidity), bundles of water molecules bound to the hydrophilic groups of the heterogeneous matrix are formed. We assume that water molecules can interact with OH-groups distributed over the external surface of crystalline cellulose fibers or located in the amorphous parts of cellulose fibers (Fig. 1). Water molecules interact with each other only inside these small water clusters without forming inter-cluster interactions (Gutina et al., 1998). Therefore, we expected to see a similar relaxation map for all NFC samples at the low hydration level. In this case, water molecules do not “sense” the sorbing matrix, but depend only on the local structural organization of water around hydration centers. Therefore, one can compare the dielectric relaxation behavior for a wide class of weakly hydrated materials showing the similar relaxation of an ice-like process at low temperatures (Feldman et al., 2014; Kurzweil-Segev et al., 2016; Ryabov, Gutina, Arkhipov, & Feldman, 2001; Vasilyeva et al., 2014).

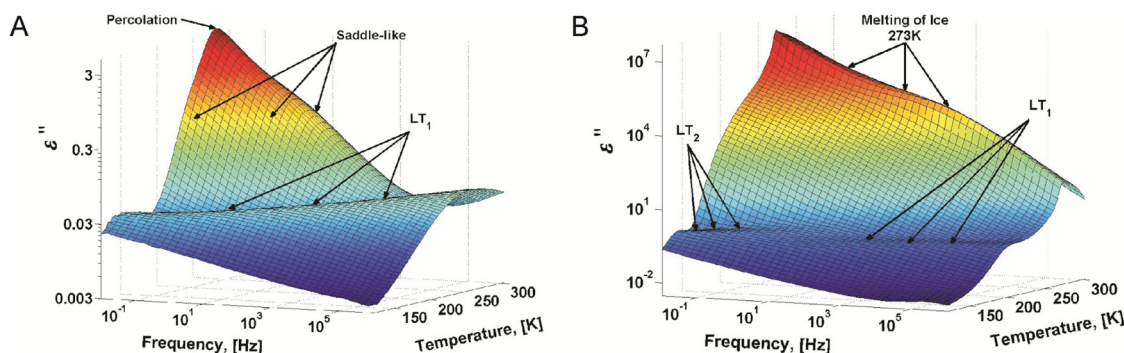


Fig. 4. Dependence of dielectric losses versus frequency and temperature for wood NFC at (a) low (29% steam humidity) and (b) high (98% steam humidity) hydration levels.

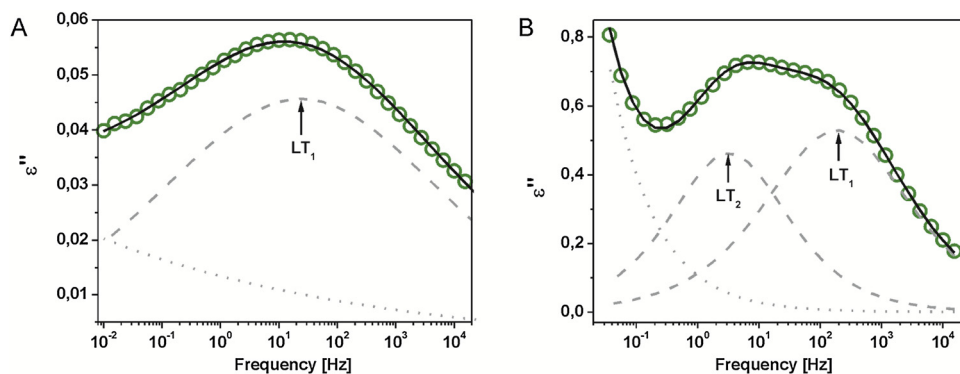


Fig. 5. The typical fit for the dielectric data (circles) of the wood NFC: low humidity sample at 168 K (left) and high humidity sample at 150 K (right). The solid lines correspond to the fit of the experimental data by Eq. 1. The separate terms of the fitting function are shown by the dashed lines (CC processes) and the dotted line (Jonscher term). (For interpretation of the references to colour in this figure legend, the reader is referred to the web version of this article.)

For a quantitative analysis of the low-temperature dielectric processes in NFC samples at a low hydration level ( $LT_1$  in Fig. 4a) a superposition of the phenomenological Cole–Cole (CC) function (Cole & Cole, 1941) and a low frequency Jonscher term was used (Greenbaum Gutina, Ben Ishai, & Feldman, 2015):

$$\epsilon^*(\omega) = \epsilon'(\omega) + i\epsilon''(\omega) = \epsilon_\infty + \frac{\Delta\epsilon}{1 + (i\omega\tau)^\alpha} + A(i\omega)^{n-1}. \quad (1)$$

Here,  $\epsilon^*(\omega)$  is the measured complex dielectric permittivity,  $\tau$  is the relaxation time;  $i^2 = -1$ ,  $\omega = 2\pi f$ ,  $f$  is the frequency. In Eq. (1)  $\Delta\epsilon = \epsilon_s - \epsilon_\infty$  is the dielectric strength with  $\epsilon_s$  and  $\epsilon_\infty$  denoting the extrapolated low-frequency and high-frequency permittivity limits, respectively; the parameter  $\alpha$  describes the symmetric broadening of the relaxation process;  $A$  is the amplitude of the Jonscher term and  $0 < n < 1$ . For a more precise fitting procedure, the data processing was performed only in the vicinity of the dielectric loss peak maximum. Thus, the Jonscher term accounts for the combined residual influence of the low frequency process. The fitting in a complex plane was carried out using in-house DATAMA software (Axelrod et al., 2004). The typical fitting for the low-temperature dielectric process in the NFC samples with low water content is presented in Fig. 5a. For the samples with high water content two Cole-Cole (CC) relaxation terms were detected ( $LT_1$  and  $LT_2$  in Fig. 4b). The typical fitting with two CC processes is presented in Fig. 5b. Note, that the second process is easily observed for the wood and flax samples whereas for the cotton NFC the process is almost completely screened beneath the  $LT_1$ .

### 3.4.2. Low water content

The temperature dependencies of the relaxation time  $\tau$  and the dielectric strength  $\Delta\epsilon$  of the low-temperature process  $LT_1$  at low water

content for NFC films fabricated from different sources are presented in Fig. 6.

For all of the samples studied, a similar temperature dynamic with an activation energy of 50 kJ/mol is observed. In addition, the increase in dielectric strength with temperature (Fig. 6b) is typical for solid materials. Such dielectric relaxation behavior is known for a wide class of weakly-hydrated heterogeneous materials that show a similar relaxation of an ice-like process at low temperatures (Cervený, Mallamace, Swenson, Vogel, & Xu, 2016; Feldman et al., 2014; Gutina, Antropova, Rysiakiewicz-Pasek, Virnik, & Feldman, 2003; Khodadadi, Pawlus, & Sokolov, 2008; Khodadadi, Curtis, & Sokolov, 2011; Ngai, Capaccioli, Ancherbak, & Shinyashiki, 2011; Ryabov et al., 2001; Vasilyeva et al., 2014).

### 3.4.3. High water content

As mentioned above, for the high water content samples two Cole-Cole (CC) relaxation processes were detected in all of the samples ( $LT_1$  and  $LT_2$  in Fig. 4b). Note that the second process is clearly observed for wood and flax samples while for the cotton NFC the process is almost completely screened by the  $LT_1$ .

The temperature dependencies of the relaxation times  $\tau_1$  and  $\tau_2$  for all NFCs with high water content are shown in Fig. 7 (left). For the wood and flax samples the relaxation time  $\tau_2$  demonstrates the Arrhenius behavior with an activation energy of around 45 kJ/mol, similar to the behavior observed in hydrated collagen and elastin, which was identified with diffusion defects in the bulk ice (Gainaru, Fillmer, & Bohmer, 2009; Kurzweil-Segev, Popov, Sagit et al., 2017; Popov et al., 2015). Therefore, the second relaxation process in these materials,  $LT_2$ , detected at high water content can be assigned to ice Ih. At the same time, the second process in the cotton sample is faster and demonstrates

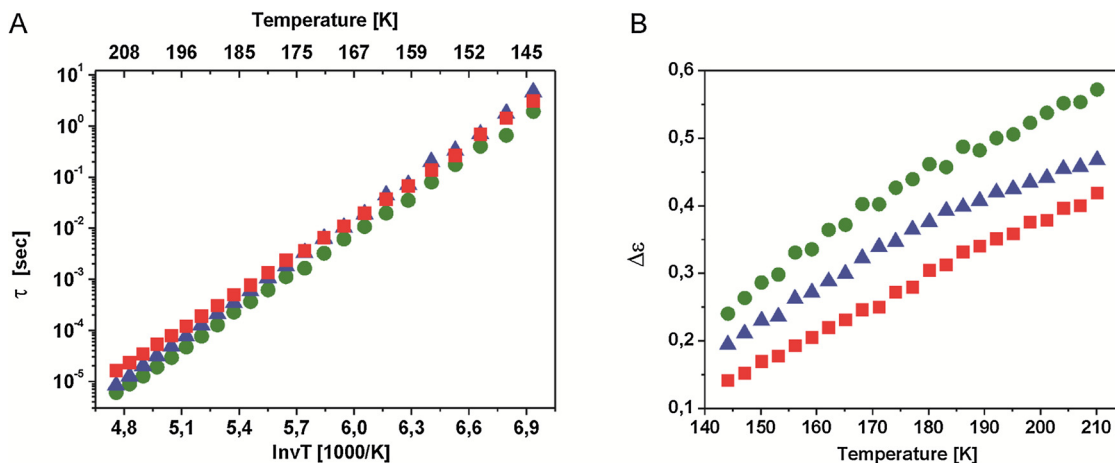
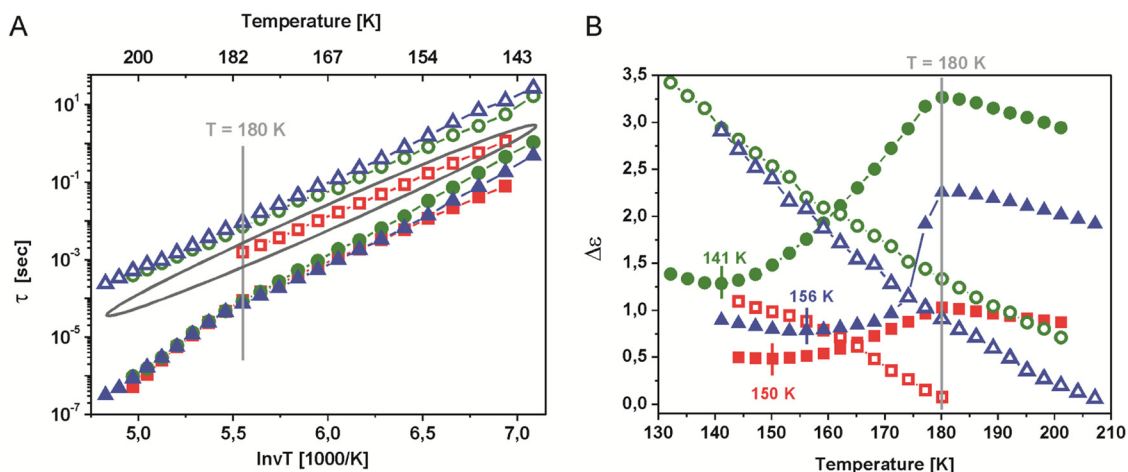


Fig. 6. Relaxation time  $\tau$  of the  $LT_1$  process in Arrhenius coordinates (left) and dielectric strength  $\Delta\epsilon$  (right) for NFC films of different plant origins at low water content: Cotton (red squares), wood (green circles) and flax (blue triangles). (For interpretation of the references to colour in this figure legend, the reader is referred to the web version of this article.)



**Fig. 7.** Temperature dependencies of relaxation times (left) and dielectric strength (right) for NFC samples with high water content at low temperatures. Full symbols correspond to the  $LT_1$  process, open ones relate to the  $LT_2$  process. The position of the  $LT_1$  process for the samples with low water content is shown within the ellipse. Red squares denote the cotton sample, green circles denote the wood and blue triangles denote the flax, correspondingly. (For interpretation of the references to colour in this figure legend, the reader is referred to the web version of this article.)

a behavior similar to the  $LT_1$ , typical for weakly hydrated materials. Thus, no crystallization of water occurs in the humid cotton sample and only small ice-like structures of hydrated water are present. In the wood and the flax samples, the dielectric response of these ice-like structures is screened by the strong dielectric contribution of the ice.

The temperature dependence of relaxation time  $\tau_1$  for all highly-hydrated NFC samples demonstrates a dynamic crossover at around  $T = 180$  K. Below the crossover point, the activation energy of this process again approaches 50 kJ/mol. This confirms the dipole-ordered ice-like character of this relaxation process. However, at high temperatures the slope of this curve increases sharply, indicating changes in the nature of this process. Since a reliable fitting analysis at temperatures higher than 213 K could not be provided, it is difficult to determine the type of relaxation behavior for this process. However, the dynamics of confined water in porous materials with different pore sizes has been studied previously and a similar crossover has been observed in high water content materials (Cervený et al., 2016; Ngai et al., 2011; Rosenstihl, Kämpff, Sattigm, & Vogel, 2015; Sjöström, Swenson, Bergman, & Kittaka, 2008). This process follows the Vogel-Fulcher-Tammann (VFT) temperature dependence that is typical for glass-forming liquids (Khodadadi, Malkovskiy, Kisliuk, & Sokolov, 2010). A possible explanation for the existence of glass-forming liquid in super-cooled NFC films is that at high hydration levels water molecules cover the fibril's surface to form a complete water layer, i.e. a conjoined water cluster, which behaves like a super-cooled liquid at low temperatures. The adsorbed water "dissolves" the surface OH and  $CH_2OH$  groups attached to carbohydrate rings and altogether they form a saturated solution at the fibril's outer surfaces as well as within the amorphous regions. Taking into account the mobility of hydroxyl groups, especially the hydroxymethyl groups, and the cross-interactions of water molecules with each other through these groups, we view these water-hydroxyl complexes as a saturated glass-forming liquid.

Compared with the low hydrated NFC samples, it is evident that at the high hydration level, the relaxation time of the hydrated water at low temperatures (the  $LT_1$  process) becomes faster. Therefore, we assume that these ice-like structures carry more defects than those formed by small bundles of water around the hydrophilic centers. The polarity of the environment close to these centers strongly influences the formation of water clusters around them, and leads to more ordered water structures, an increase of the hydrogen bond energy and, therefore, to the slowing down of the  $LT_1$  relaxation process. Thus, the increase in water quantity at the outer fibril surfaces leads to the formation of additional defects in the ice-like structures, thus promoting the

relaxation to occur.

For a better understanding of the dynamics and structure of water in the NFC films at high water content, we analyzed the dielectric strength of the  $LT_1$  process. If the temperature dependence of the relaxation times reflects the dynamics of hydrated water, the static permittivity  $\epsilon_s$  of this process reflects the structural aspects of water polarization and dipole-dipole interactions. It is well known that the entropy of a system depends on its static permittivity (Fröhlich, 1958). In the case of a weak temperature dependency of  $\epsilon_\infty$  we can write

$$S = S_0(T) + \frac{\partial \epsilon_s}{\partial T} \frac{E^2}{8\pi} \approx S_0(T) + \frac{\partial \Delta \epsilon}{\partial T} \frac{E^2}{8\pi} \quad (2)$$

Here,  $S_0(T)$  is the entropy of the system in the absence of an electric field  $E$ . According to this equation we can see that at  $\partial \Delta \epsilon / \partial T < 0$  the entropy decreases. This behavior is typical for dipole-disordered systems such as liquids or gasses. On the other hand, when  $\partial \Delta \epsilon / \partial T > 0$ , the entropy increases and corresponds to that of dipole-ordered systems.

The temperature dependence of dielectric strength for the  $LT_1$  process reveals three different intervals for all NFC samples (Fig. 7). At the lowest temperatures, the dielectric strength  $\Delta \epsilon$  of the quenched samples demonstrates a liquid-like disordered behavior, which is typical for super-cooled liquids. Under heating,  $\Delta \epsilon(T)$  starts to exhibit a dipole-ordered behavior. Note, the temperature points at which the dielectric strength alters the sign of its slope are 141 K, 150 K and 156 K for wood, cotton and flax, respectively. This clearly indicates the onset of a disorder-to-order transition, that most probably depends on material properties. A further increase of temperature leads to another sharp alteration in the  $\Delta \epsilon$  temperature behavior at about 180 K for all samples studied - from the solid-like (ordered) to the liquid-like (disordered) type of hydrated water structures. Furthermore, it corresponds exactly to the crossover temperature and makes a case for the universality of such sharp alterations in the system (Cervený et al., 2016; Khodadadi et al., 2010).

Taking into account the considerations discussed above, we can propose the following generalized scheme of water structure and dynamics transitions in hydrated NFC films (see Fig. 8):

A. Upon being exposed to the high humidity atmosphere at room temperature, the NFC films start to adsorb water molecules near the primary hydrated sites, i.e. hydroxyl groups, in the form of spatially-separated water clusters (this stage of water adsorption is clearly seen at low humidity). Subsequently, these clusters are covered by additional water layers, leading to the formation of a saturated water solution where the flexible hydroxyl groups play the role of a solute. Furthermore, additional sorption leads to the disruption of the

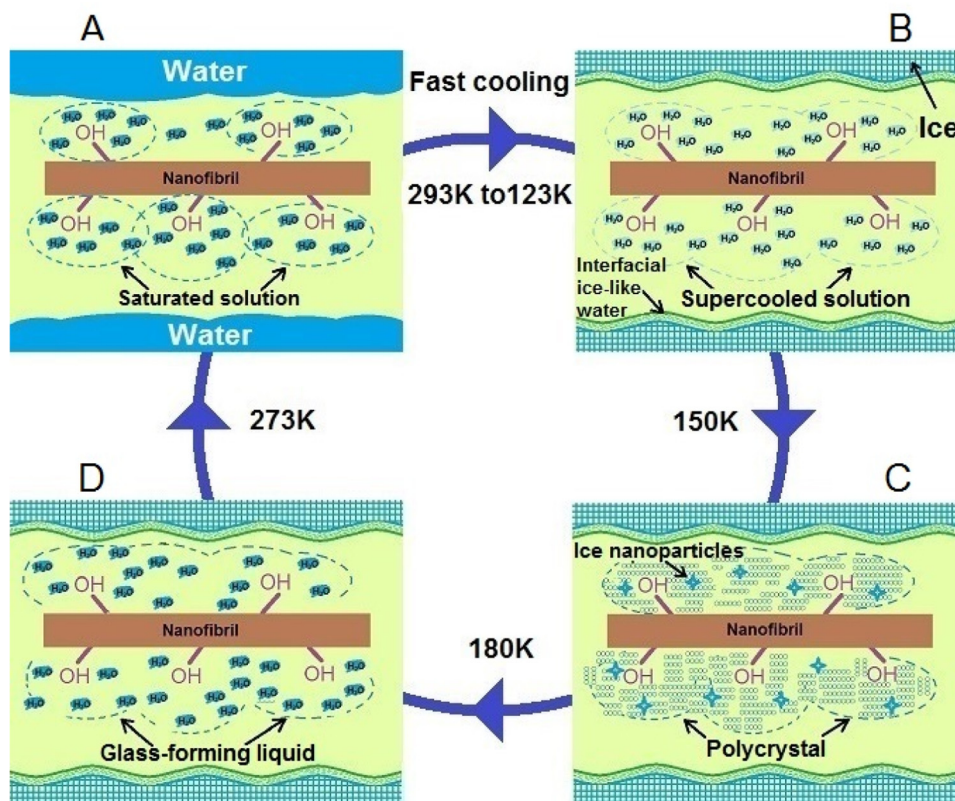


Fig. 8. Schematic representation of the water structures at low temperatures in the NFC hydrated films.

hydrogen bonds formed by nanofibrils at their intersections in the sample, thus resulting in a swelling of the film (Belbekhouche et al., 2011). Therefore, two general structures of adsorbed water can be distinguished – the saturated water solution in the vicinity of the NFC surface and bulk water (Fig. 8A).

B. The fast cooling down of the hydrated NFC films to 123 K results in the formation of a super-cooled phase from the saturated glass-forming solution. The cooling is rapid enough to prevent crystallization of the saturated water-hydroxyl solution. However, this fast cooling is not enough to prevent the formation of ice from the bulk water inside the heterogeneous structure of the films. An intermediate ice-like interfacial water structure is also formed.

C. On heating, the super-cooled solution undergoes cold crystallization at around 150 K. We detect this cold crystallization due to the change in the slope of the dielectric strength at 141 K, 150 K and 156 K for wood, cotton and flax, respectively. This confirms that the cold crystallization depends strongly on the nature of the plant. The process leads to the formation of solid poly-crystalline structures of the glass-forming liquid accompanied by the creation of small, uniformly-sized confined ice particles distributed between crystallites.

D. It is well known that under confinement conditions the freezing/melting of water/ice differs from that of the bulk and behaves according to the Gibbs-Thompson relationship (Kurzweil-Segev et al., 2016; Moore, Allen, & Molinero, 2012; Schmidt, Hansen, Stoecker, Akporiaye, & Ellestad, 1995). The temperature 180 K corresponds to the melting of ice particles confined into 1–2 nm size volumes (Kurzweil-Segev et al., 2016; Kurzweil-Segev et al., 2016; Kurzweil-Segev, Popov, Eisenberg et al., 2017), which are reasonable for our systems. Thus, we can conclude that while the small ice crystals simultaneously melt at this particular temperature, the poly-crystalline structure of the water “solution” softens and transforms into an amorphous regular glass-former liquid. Further heating melts the bulk ice structures at 273 K.

In summary, the investigated NFCs of different plant sources vary in the crystallinity index, the diameter of nanofibrils and the resulting

morphology of the NFC films (sections 3.1 and 3.2). Furthermore, the amount of adsorbed water and its structure strongly depends on the origin of the material (sections 3.3 and 3.4). The amount of adsorbed water is inversely proportional to the diameter of the nanofibrils. Additionally, the distribution of adsorbed water over the saturated solution and the bulk water depends on the NFC origin. We consider the presence or absence of the adsorbed water to be of major importance for the technological application of NFC materials. Dielectric spectroscopy proves to be a useful tool to differentiate the adsorbed water structure and, hence, the morphology of NFCs.

#### 4. Conclusions

The cellulose-water interactions are of crucial fundamental and technological importance because the hydration determines the structural stability and mechanical properties of cellulose. The present study expands the knowledge of the interplay between nanofibrillated cellulose films and hydrated water. The cellulose materials from three different plant sources of technological importance, i.e. cotton, wood and flax, were compared with respect to the state of hydrated water at low and high water content. At low water content (28% relative humidity), the adsorbed water forms small isolated clusters on the surface of the nanofibrils. Under these conditions, the state of the adsorbed water within the three samples studied was indistinguishable for dielectric spectroscopy. At high water content (98% relative humidity), some of the hydrated water covers the surface of the nanofibrils, forming a continuous water shell that represents a saturated “solution” of available surface hydroxyl groups of cellulose. This type of water does not freeze under fast cooling down to 123 K. Partially adsorbed water possesses the properties of bulk, thus freezing as regular ice. The films of three NFCs studied demonstrate different abilities to retain hydrated and bulk-like water in their volume. This discrepancy seems to be determined by the peculiarity of a swelling process in the films, which in turn is due to the morphology difference of the porous NFC films. Thus,

the water present in all cellulose materials displays both the overall and specific marks of the NFCs' structure. The dielectric spectroscopy of hydrated water provides a universal approach to characterize the generalized structural properties of cellulose samples.

## Acknowledgements

The authors would like to thank Dr. Vladislav Lirtsman for his technical assistance. The contribution of IL, OM and YZ was supported by financial assistance from the government assignment of Federal Research Center "Kazan Scientific Center of Russian Academy of Sciences".

## References

- Abou-Sekkina, M., Sakran, M., & Saafan, A. (1986). Development of correlations among the spectral, structural, and electrical properties and chemical treatment of Egyptian cotton fabric strips. *Ind. Chem. Prod. Res. Develop.* 25(4), 676–680.
- Alemdar, A., & Sain, M. (2008). Biocomposites from wheat straw nanofibers: Morphology, thermal and mechanical properties. *Composites Science and Technology*, 68(2), 557–565.
- Arai, C., Hosaka, S., & Murase, R. (1976). Measurements of relative humidity of saturated aqueous salt solutions. *Journal of Chemical Engineering of Japan*, 9(4), 328–330.
- Axelrod, N., Axelrod, E., Gutina, A., Puzenko, A., Ben Ishai, P., & Feldman, Y. (2004). Dielectric spectroscopy data treatment: I. Frequency domain. *Measurement Science & Technology*, 15, 755–764.
- Belbekhouche, S., Bras, J., Siqueira, G., Chappey, C., Lebrun, L., Khelifi, B., ... Dufresne, A. (2011). Water sorption behavior and gas barrier properties of cellulose whiskers and microfibrils films. *Carbohydrate Polymers*, 83, 1740–1748.
- Bone, S., & Pethig, R. (1982). Dielectric studies of the binding of water to lysozyme. *Journal of Molecular Biology*, 157(3), 571–575.
- Bras, D. L., Strømme, M., & Mihranyan, A. (2015). Characterization of dielectric properties of nanocellulose from wood and algae for electrical insulator applications. *The Journal of Physical Chemistry B*, 119(18), 5911–5917.
- Cervený, S., Mallamace, F., Swenson, J., Vogel, M., & Xu, L. (2016). Confined water as model of supercooled water. *Chemical Reviews*, 116(13), 7608–7625.
- Charreau, H., Foresti, M. L., & Vázquez, A. (2013). Nanocellulose patents trends: A comprehensive review on patents on cellulose nanocrystals, microfibrillated and bacterial cellulose. *Recent Patents on Nanotechnology*, 7(1), 56–80.
- Chen, J., Guo, J., Meng, X., Peng, J., Sheng, J., Xu, L., ... Wang, E.-G. (2014). An unconventional bilayer ice structure on a NaCl(001) film. *Nature Communications*, 5, 5232.
- Chinga-Carrasco, G. (2011). Cellulose fibres, nanofibrils and microfibrils: The morphological sequence of MFC components from a plant physiology and fibre technology point of view. *Nanoscale Research Letters*, 6, 1–10.
- Cole, K. S., & Cole, R. H. (1941). Dispersion and absorption in dielectrics I. Alternating current characteristics. *J Chem Phys Eng Data*, 9, 341–351.
- Dagnon, K. L., Shanmuganathan, K., Weder, C., & Rowan, S. J. (2012). Water-triggered Modulus changes of cellulose nanofiber nanocomposites with hydrophobic polymer matrices. *Macromolecules*, 45, 4707–4715.
- Ehre, D., Lavert, E., Lahav, M., & Lubomirsky, I. (2010). Water freezes differently on positively and negatively charged surfaces of pyroelectric materials. *Science*, 327(5966), 672–675.
- Einfeldt, J., & Kwasniewski, A. (2002). Characterization of different types of cellulose by dielectric spectroscopy. *Cellulose*, 9, 225–238.
- Einfeldt, J., Meißner, D., & Kwasniewski, A. (2003). Contributions to the molecular origin of the dielectric relaxation processes in polysaccharides – The high temperature range. *J. Non-Cryst. Solids*, 320, 40–55.
- Feldman, Y., Ermolina, I., & Hayashi, Y. (2003). Time domain dielectric spectroscopy study of biological systems. *IEEE Transactions on Dielectrics and E*, 10(5), 728–775.
- Feldman, Y., Puzenko, A., Ben Ishai, P., & Gutina Greenbaum, A. (2014). The dielectric response of interfacial water - from the ordered structures to the single hydrated shell. *Colloids & Polymers*, 29, 1923–1932.
- Feldman, Y., Puzenko, A., & Ryabov, Y. (2006). *Dielectric relaxation phenomena in complex materials. In fractals, diffusion, and relaxation in disordered complex systems*. John Wiley & Sons, Inc1–125.
- Fengel, D. (1971). Ideas on the ultrastructural organization of the cell wall components. *J Polym Sci, Part C, Polymer Symposia*, 36, 383–392.
- Fröhlich, H. (1958). *Theory of dielectrics; dielectric constant and dielectric loss* (2d ed.). Oxford: Clarendon Press.
- Gainaru, C., Fillmer, A., & Bohmer, R. (2009). Dielectric response of deeply supercooled hydration water in the connective tissue proteins collagen and elastin. *The Journal of Physical Chemistry B*, 113, 12628–12631.
- Gallo, P., Rovere, M., & Chen, S. H. (2012). Water confined in MCM-41: A mode coupling theory analysis. *Journal of Physics Condensed Matter*, 24(6), 064109.
- Greenbaum Gutina, A., Ben Ishai, P., & Feldman, Y. (2015). Analyses of experimental data and fitting problems. In V. Raicu, & Y. Feldman (Eds.). *Dielectric relaxation in biological systems* (pp. 170–189). Oxford, UK: Oxford University Press.
- Gutina, A., Antropova, T., Rysiakiewicz-Pasek, E., Virnik, K., & Feldman, Y. (2003). Dielectric relaxation in porous glasses. *Microporous and Mesoporous Materials*, 58(3), 237–254.
- Gutina, A., Axelrod, E., Puzenko, A., Rysiakiewicz-Pasek, E., Kozlovich, N., & Feldman, Y. (1998). Dielectric relaxation of porous glasses. *J. Non-Crystalline Sol.* 235-237, 302–307.
- Heux, L., Dinand, E., & Vignon, M. R. (1999). Structural aspects in ultrathin cellulose microfibrils followed by <sup>13</sup>C CP-MAS NMR. *Carbohydrate Polymers*, 40(2), 115–124.
- Iwamoto, S., Nakagaito, A. N., & Yano, H. (2007). Nano-fibrillation of pulp fibers for the processing of transparent nanocomposites. *Applied Physics A, Materials Science & Processing*, 89(2), 461–466.
- Jafarpour, G., Dantras, E., Boudet, A., & Lacabanne, C. (2007). Study of dielectric relaxations in cellulose by combined DDS and TSC. *Journal of Non-crystalline Solids*, 353, 4108–4115.
- Jafarpour, G., Roig, F., Dantras, E., Boudet, A., & Lacabanne, C. (2009). Influence of water on localized and delocalized molecular mobility of cellulose. *J. Non-Cryst. Solids*, 355, 1669–1672.
- Khodadadi, S., Curtis, J. E., & Sokolov, A. P. (2011). Nanosecond relaxation dynamics of hydrated proteins: Water versus protein contributions. *The Journal of Physical Chemistry B*, 115, 6222–6226.
- Khodadadi, S., Malkovskiy, A., Kisliuk, A., & Sokolov, A. P. (2010). A broad glass transition in hydrated proteins. *Biochimica et Biophysica Acta*, 1804, 15–19.
- Khodadadi, S., Pawlus, S., & Sokolov, A. P. (2008). Influence of hydration on protein dynamics: Combining dielectric and neutron scattering spectroscopy data. *The Journal of Physical Chemistry B*, 112(45), 14273–14280.
- Kremer, F., & Schonhals, A. (2003). *Broadband dielectric spectroscopy*. Berlin: Springer-Verlag.
- Kubicki, J. D., Yang, H., Sawada, D., O'Neill, H., Oehme, D., & Cosgrove, D. (2018). The shape of native plant cellulose microfibrils. *Scientific Reports*, 8, 1–10.
- Kurzweil-Segev, Y., Gutina, A. G., Popov, I., Golodnitsky, D., & Feldman, Y. (2016). The role of the confined water in the dynamic crossover of a hydrated Lysozyme powders. *PCCP*, 18, 10992–10999.
- Kurzweil-Segev, Y., Popov, I., Eisenberg, I., Yochelis, S., Keren, N., Paltiel, Y., & Feldman, Y. (2017). Confined Water Dynamics in Hydrated photosynthetic pigment protein complex. *Physical Chemistry Chemical Physics : PCCP*, 19(41), 28063–28070.
- Kurzweil-Segev, Y., Popov, I., Sagit, I., Solomonov, I., & Feldman, Y. (2017). The mechanism of the dielectric relaxation of the hydration water in native collagen fibrils. *The Journal of Physical Chemistry B*, 121(21), 5340–5346.
- Lang, E. W., & Ludemann, H. D. (1982). Anomalies of liquid water. *Angewandte Chemie-International Edition in English*, 21(5), 315–329.
- Lavoine, N., Deslozes, I., Dufresne, A., & Bras, J. (2012). Microfibrillated cellulose - its barrier properties and applications in cellulosic materials: A review. *Carbohydrate Polymers*, 90(2), 735–764.
- Lu, J., Askeland, P., & Drzal, L. T. (2008). Surface modification of microfibrillated cellulose for epoxy composite applications. *Polymer*, 49(5), 1285–1296.
- Martin, D. R., & Matyushov, D. V. (2015). Dipolar nanodomains in protein hydration shells. *The Journal of Physical Chemistry Letters*, 6(3), 407–412.
- Moore, E. B., Allen, J. T., & Molinero, V. (2012). Liquid-ice coexistence below the melting temperature for water confined in hydrophilic and hydrophobic nanopores. *The Journal of Physical Chemistry C*, 116, 7507–7514.
- Ngai, K. L., Capaccioli, S., Ancherbak, S., & Shinyashiki, N. (2011). Resolving the ambiguity of the dynamics of water and clarifying its role in hydrated proteins. *Philosophical Magazine*, 91, 1809–1835.
- Nilsson, M., Frenning, G., Gråsjö, J., Alderborn, G., & Strømme, M. (2006). Conductivity percolation in loosely compacted microcrystalline cellulose: An in situ study by dielectric spectroscopy during densification. *The Journal of Physical Chemistry B*, 110, 20502–20506.
- Nisizawa, K. (1973). Mode of action of cellulases. *Journal of Fermentation Technology*, 51, 267–304.
- Nixon, B. T., Mansouri, K., Singh, A., Du, J., Davis, J. K., Lee, J. G., ... Haigler, C. H. (2016). Comparative structural and computational analysis supports eighteen cellulose synthases in the plant cellulose synthesis complex. *Scientific Reports*, 6, 1–10.
- Pal, S. K., Peon, J., & Zewail, A. H. (2002). Biological water at the protein surface: Dynamical solvation probed directly with femtosecond resolution. *Proceedings of the National Academy of Sciences*, 99(4), 1763–1768.
- Pérez, S., & Mazeau, K. (2005). Conformations, structures, and morphologies of celluloses. In S. Dumitriu (Ed.). *Polysaccharides: Structural diversity and functional versatility*. Marcel Dekker.
- Popov, I., Puzenko, A., Khamzin, A., & Feldman, Y. (2015). *The dynamic crossover in dielectric relaxation behavior of ice Ih*. *PCCP*, 17, 1489–1497.
- Puzenko, A., Kozlovich, N., Gutina, A., & Feldman, Y. (1999). Determination of pore fractal dimensions and porosity of silica glasses from the dielectric response at percolation. *Physical Review B*, 60(20), 1–10.
- Rachocki, A., Markiewicz, E., & Tritt-Goc, J. (2005). Dielectric relaxation in cellulose and its derivatives. *Acta Physica Polonica A*, 108, 137–145.
- Rankoana, S. A. (2016). Sustainable Use and Management of Indigenous Plant Resources: A Case of Mantheding Community in Limpopo Province, South Africa. *Sustainability*, 8, 221–234.
- Reiter, G. F., Deb, A., Sakurai, Y., Itou, M., Krishnan, V. G., & Paddison, S. J. (2013). Anomalous ground state of the electrons in Nanoconfined Water. *Physical Review Letters*, 111(3), 036803.
- Richardson, J. M., & Malthus, R. S. (1955). Salts for static control of humidity at relatively low levels. *Journal of Chemical Technology & Biotechnology*, 5(10), 557–567.
- Roig, F., Dantras, E., Dandurand, J., & Lacabanne, C. (2011). Influence of hydrogen bonds on glass transition and dielectric relaxations of cellulose. *Journal of Physics D: Applied Physics*, 44, 045403–045408.
- Rosenstihl, M., Kämpff, K., Sattigm, K., & Vogel, M. (2015). Dynamics of interfacial water. *Journal of Non-crystalline Solids*, 407, 449–458.
- Rupley, J. A., Gratton, E., & Careri, G. (1983). Water and globular proteins. *Trends in Biochemical Sciences*, 8(1), 18–22.

- Ryabov, Y., Gutina, A., Arkhipov, V., & Feldman, Y. (2001). Dielectric relaxation phenomena of water absorbed in porous glasses. *The Journal of Physical Chemistry B*, *105*, 1845–1850.
- Schmidt, R., Hansen, E. W., Stoecker, M., Akporiaye, D., & Ellestad, O. H. (1995). Pore Size Determination of MCM-51 Mesoporous Materials by means of <sup>1</sup>H NMR Spectroscopy, N<sub>2</sub> adsorption, and HREM. A Preliminary Study. *Journal of the American Chemical Society*, *117*(14), 4049–4056.
- Siqueira, G., Bras, J., & Dufresne, A. (2010). Cellulosic bionanocomposites: A review of preparation properties and applications. *Polymers*, *2*, 728–765.
- Sjöström, J., Swenson, J., Bergman, R., & Kittaka, S. (2008). Investigating hydration dependence of dynamics of confined water: Monolayer, hydration water and Maxwell – Wagner processes. *The Journal of Chemical Physics*, *128*, 154503.
- Sousa, M., Brás, A. R., Veiga, H. I. M., Ferreira, F. C., Pinho, M. N., Correia, N. T., & Dionísio, M. (2010). Dynamical characterization of a cellulose acetate polysaccharide. *The Journal of Physical Chemistry B*, *114*, 10939–10953.
- Stokely, K., Mazza, M. G., Stanley, H. E., & Franzese, G. (2010). Effect of hydrogen bond cooperativity on the behavior of water. *Proceedings of the National Academy of Sciences of the United States of America*, *107*(4), 1301–1306.
- Suzuki, Y., Duran, H., Steinhart, M., Kappl, M., Butt, H. J., & Floudas, G. (2015). Homogeneous nucleation of predominantly cubic ice confined in Nanoporous Alumina. *Nano Letters*, *15*(3), 1987–1992.
- Suzuki, Y., Steinhart, M., Butt, H. J., & Floudas, G. (2015). Kinetics of ice nucleation confined in Nanoporous Alumina. *The Journal of Physical Chemistry B*, *119*(35), 11960–11966.
- Tanaka, H. (2013). Importance of many-body orientational correlations in the physical description of liquids. *Faraday Discussions*, *167*, 9–76.
- Vasilyeva, M. A., Gusev, Y. A., Shtyrlin, V. G., Greenbaum Gutina, A., Puzenko, A., Ben Ishai, P., & Feldman, Y. (2014). Dielectric relaxation of water in natural layer aluminosilicates. *Clays and Clay Minerals*, *62*, 62–73.
- Viet, D., Beck-Candanedo, S., & Gray, D. G. (2007). Dispersion of cellulose nanocrystals in polar organic solvents. *Cellulose*, *14*, 109–113.
- Wada, M., Okano, T., & Sugiyama, J. (1997). Synchrotron-radiated X-ray and neutron diffraction study of native cellulose. *J. Cellulose*, *4*(3), 221–232.
- Wada, M., Sugiyama, J., & Okano, T. (1993). Native celluloses on the basis of two crystalline phase (I $\alpha$ /I $\beta$ ) system. *Journal of Applied Polymer Science*, *49*, 1491–1496.
- Zhao, H., Chen, Z., Du, X., & Chen, L. (2019). Contribution of different state of adsorbed water to the sub-T<sub>g</sub> dynamics of cellulose. *Carbohydrate Polymers*, *210*, 322–331.